Applied Surface Science 400 (2017) 14–23

Contents lists available at ScienceDirect

Applied Surface Science

journal homepage: www.elsevier.com/locate/apsusc

Full Length Article

Biofunctionalization of carbon nanotubes/chitosan hybrids on Ti implants by atom layer deposited ZnO nanostructures

Yizhou Zhu[a], Xiangmei Liu[a], Kelvin W.K. Yeung[b], Paul K. Chu[c], Shuilin Wu[a,*]

[a] Hubei Collaborative Innovation Center for Advanced Organic Chemical Materials, Ministry-of-Education Key Laboratory for the Green Preparation and Application of Functional Materials, Hubei Key Laboratory of Polymer Materials, School of Materials Science & Engineering, Hubei University, Wuhan 430062, China

[b] Division of Spine Surgery, Department of Orthopaedics & Traumatology, Li Ka Shing Faculty of Medicine, The University of Hong Kong, Pokfulam, Hong Kong, China

[c] Department of Physics & Materials Science, City University of Hong Kong, Tat Chee Avenue, Kowloon, Hong Kong, China

ARTICLE INFO

Article history:
Received 15 October 2016
Received in revised form
13 December 2016
Accepted 19 December 2016
Available online 21 December 2016

Keywords:
Carbon nanotubes
ZnO
Hybrid coating
Antibacterial
Surface biofunctionalization

ABSTRACT

One-dimensional (1D) nanostructures of ZnO using atomic layer deposition (ALD) on chitosan (CS) modified carbon nanotubes (CNTs) were first introduced onto the surfaces of biomedical implants. When the content of ZnO is not sufficient, CNTs can strengthen the antibacterial activity against *E. coli* and *S. aureus* by 8% and 39%, respectively. CS can improve the cytocompatibility of CNTs and ZnO. The amount of Zn content can be controlled by changing the cycling numbers of ALD processes. This hybrid coating can not only endow medical implants with high self-antibacterial efficacy against Escherichia coli (*E. coli*) and Staphylococcus aureus (*S. aureus*) of over 73% and 98%, respectively, but also regulate the proliferation and osteogenic differentiation of osteoblasts by controlling the amount of ZnO.

1. Introduction

Titanium (Ti) and its alloys are widely used as implant materials in the dental and orthodontic fields because of their excellent biocompatibility, osteoconductivity and mechanical properties [1,2]. However, infection associated with implants has already become increasingly serious clinical problems, such as prolonged hospitalization, implant failure, and even death [3,4]. In addition, the bioinert nature is the instinctive defect of Ti-based implants [5]. Therefore, researchers have attempted to modify the Ti surface with nanostructure or coatings to improve osteogenesis inducing ability as well as inhibit bacterial colonization [6–8].

Carbon nanotubes (CNTs) attract attention of many researchers due to their unique properties, such as ultrahigh surface areas (up to 1587 m^2/g) [9], excellent mechanical properties (average Young's modulus of Y = 1–1.8 Ta for multiwalled carbon nanotubes) [10] and thermal stability (the sublimation temperature can be over 2900 K) [11]. Hence, CNTs have attracted broad research interest including drug delivery, biological imaging, biological scaffold and biosensing. CNTs have been reported to exhibit cytotoxicity over a wide range of bacteria including human pathogens such as *Escherichia coli* (*E. coli*) [12], *Salmonella typhimurium* [13], *Bacillus subtilis, Staphylococcus aureus* (*S. aureus*), *Micrococcus lysodeikticus* [14] and *Streptococcus mutans* [15]. Different antibacterial mechanisms of CNTs have been proposed. Several studies have reported that CNTs exhibit antibacterial activity by physical puncturing and physical contact with the bacterial cell surface [16]. Other researchers also reveal that CNTs can produce reactive oxygen species (ROS) and increase oxidative stress, killing bacteria by damaging cell membrane [17]. In addition, CNTs have been reported to have a promoting effect on osteoblast differentiation [18]. Price et al. has been first reported the smaller diameter carbon nanofibers could increase osteoblast adhesion and decrease the adhesion of osteoblast-competitive cell line (fibroblasts, chondrocytes, and smooth muscle cells) [19]. Carbon nanofibers can also improve the function of osteoblast and enhance bonding of orthopedic implants to juxtaposed bone [20].

Although it has been reported that CNTs coated Ti can exhibit a greater cell adhesion [18] and better antibacterial activity than non-coated Ti, some studies have reported that pristine CNTs can inhibit cell proliferation [21], improve the level of oxidative stress

* Corresponding author.
E-mail addresses: shuilin.wu@gmail.com, shuilin.wu@hubu.edu.cn, sxwsl1976@163.com (S. Wu).

http://dx.doi.org/10.1016/j.apsusc.2016.12.158
0169-4332/

in cell [22,23] and even cause cell death [24,25]. Chitosan (CS) has been used in many coating systems due to its biocompatibility, biodegradability, non-toxicity, ability to link to and deliver growth factors and excellent film-forming property [26,27]. To improve the biocompatibility of CNTs, oxygenous groups were first introduced onto the surface of CNTs and then grafted with CS [28–30].

Zinc oxide (ZnO) has been widely used as a broad-spectrum bactericidal agent, which can resist almost all bacteria [31,32]. Zinc ion and ROS generated from ZnO were considered to be the two major factors to inhibit bacteria [33,34]. In addition, Zinc is one of the trace elements which can influence the proliferation and the differentiation of the osteoblasts [35,36].

Atomic Layer Deposition (ALD) was first developed by Suntola and Antson in 1970s [37]. Based on two successive and cyclic sequentially self-limiting half-reactions, this technique can be used to produce thin films and overlayers in a layer-by-layer mode in nanometer range on substrate surfaces. Compared to other vapor deposition methods, ALD can precisely control the thickness of deposited film at the Ångstrom or monolayer level [38]. In addition, its low deposition temperature (even down to room temperature), allowing this technique applicable for heat-sensitive substrates (such as polymer and biomaterials) [39].

Here, multiwalled carbon nanotubes (CNTs) were first treated with acid and then modified with chitosan. Subsequently, the carbon nanotubes/chitosan composites (CNTs/CS) were deposited onto the alkali-heat-treated Ti (named AHT) surface by electrophoretic deposiotn (EPD). ZnO nanofilms with different contents of ZnO were deposited by ALD. This hybrid coating on Ti is expected to combine the positive properties of CNTs, chitosan, and ZnO to achieve more effective antibacterial efficiency as well as tunable cell behaviors. The biofunctionalization mechanism can be schematically illustrated in Scheme 1.

2. Materials and methods

2.1. Sample preparation

2.1.1. Pretreatment of Ti samples

Ti disks with a diameter of 6 mm and a thickness of 2.5 mm were first mechanically polished using various grades of abrasive carbide papers. Subsequently, the physical polished samples were then cleaned with ethyl alcohol and deionized water via sonication. These samples were dried in air, followed by chemical etching in mixed solution of $H_2O/HNO_3/HF$ with volume ratio of 5:4:1 according to the literature [40], and then rinsed with deionized water several times. Alkali-heat-treatment was introduced on etched Ti surface with 4M NaOH at 80 °C for 90 min (named AHT). These pretreated Ti disks were collected and washed using deionized water adequately, and then stored for further use.

2.1.2. Purification and functionalization of CNTs

Multiwalled CNTs with an average outer diameter of over 50 nm and a length of 10–20 μm were purchased from Chengdu organic chemicals Co. Ltd, Chinese Academy of Sciences (Chengdu, China). In order to remove carbonaceous impurities and bulk CNTs, purchased CNTs were first annealed at 450 °C in air for 90 min. After annealing, 1 g of CNTs were added into 120 mL of mix acid solution (H_2SO_4-HNO_3, v:v = 3:1) according to the literature [41], and ultrasonicated for 3 h. The mixture was stirred at room temperature for 36 h. Subsequently, the acid treated CNTs were filtered using a 0.22 μm mixed cellulose filter paper and washed thoroughly with deionized water until the pH of washings reached to 7, and then dried at 60 °C under vacuum for 24 h.

2.1.3. Electrophoretic deposition (EDP)

75 mg of chitosan (≧95%, Mw = 179.17, Aladdin) was slowly added into a mixed solution containing 145 mL of 0.1% acetic acid and 5 mL of ethanol. 150 mg of acid modified CNTs was then added into this mixture and ultrosonicated for 1 h. The obtained mixtures was then magnetically stirred (1000 r/min) for next 24 h. EPD process was maintained for 30 s with an deposition voltage of 30 V. During this course, the AHT samples and a platinum plate were used as cathode electrode and anode electrode, respectively. The distance between two electrodes was 10 mm. The obtained samples (CNTs/CS) were immediately rinsed with deionized water and then dried overnight at room temperature.

2.1.4. Atomic layer deposition of ZnO

In an ALD-ZnO process, a commercial ALD reactor (F-100-41, MNT Micro and Nanotech Co., LTD, Wuxi, China) was utilized. Diethylzinc (DEZ) and deionized water (H_2O) were used as Zn and O precursors, respectively. The temperature of the H_2O source was 35 °C and DEZ source was kept at room temperature. The delivery lines and the chamber were heated to 180 °C and 120 °C, respectively. High purity nitrogen was used as the gas carrier with a flow rate of 20 mL/min and the ALD reactor was sustained at a low level of pressure with a vacuum pump. One complete ZnO ALD cycle was carried out through the gas filling of DEZ/H_2O with a 30 ms pulse, and then followed by the purge of N_2 for 10 s to eliminate the oversupplied DEZ/H_2O and any by-products. We fabricated three different groups of samples by changing the ALD cycles of ZnO, i.e., 30, 100, and 300 cycles. For AHT/ZnO modified group, samples were named as AHT-ZnO(30), AHT-ZnO(100), AHT-ZnO(100). For CNT/CS/ZnO coated groups, samples were named as CNTs/CS-ZnO(30), CNTs/CS-ZnO(100), CNTs/CS-ZnO(300).

2.2. Surface characterization

In order to estimate the compositions of the hybrids, CNTs and CNTs/CS scraped from the substrates were characterized by thermogravimetric analysis (TGA1, Mettler-Toledo). Samples were heated from 30 to 800 °C with a heating rate of 20 °C min^{-1} in N_2 flow (40 mL/min) and N_2 as the balance gas (20 mL/min). The chemical compositions of the hybrid coatings were further determined by X-ray photoelectron spectroscopy (XPS, Escalab 250Xi) and a Fourier transform infrared spectroscopy (FTIR, NICOLET iS10) in the range from 650 to 4000 cm^{-1}. Field-emission scanning electron microscopy (FE-SEM, JSM7100F) is utilized to examine the surface topography of samples. The morphologies of CNTs/CS and ZnO with different ALD cycles scraped from Ti surface were investigated using a transmission electron microscope (TEM, Tecnai G20). Water contact angles on samples were measured using contact angle goniometer (Powereach, JC2000D2) via sessile drop method at room temperature. Average roughness of samples was examined using Atom Force Microscope (AFM, Nanoscope IIIa).

2.3. Zn-loading capacity

To evaluate the capacity of Zn-loading of hybrid nanostructures, ALD-ZnO coated samples of different cycles were immersed in 1M HNO_3 for 1 day. The amount of Zn leached to solutions was measured by inductively-coupled plasma atomic emission spectrometry (ICP-AES, Opitmal 8000).

2.4. Antibacterial assay

E. coli is a kind of Gram-negative bacterium with the largest number in intestines of many animals and humans and *S. aureus* is one of the major sources of implant-associated infection in orthopaedics [42]. These two kinds of bacteria were chosen to

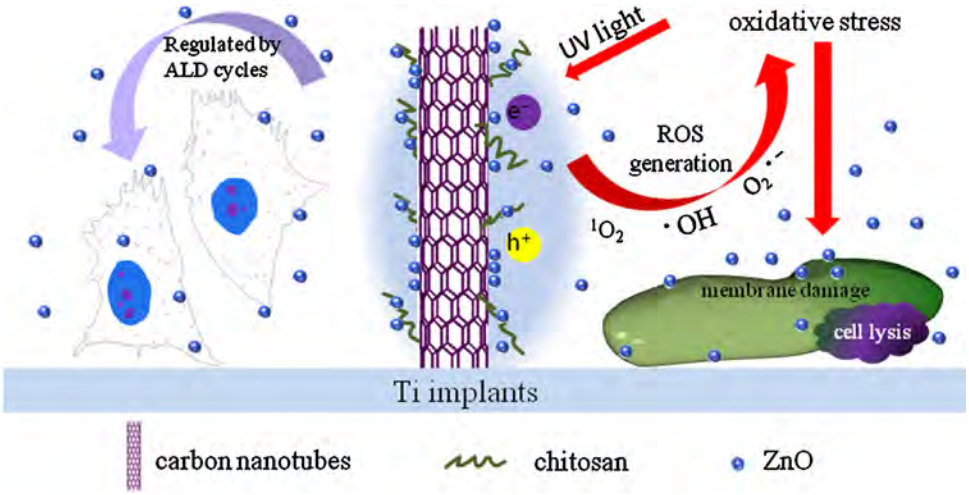

Scheme 1. The biofunctionalization mechanism of ZnO/chitosan/carbon nanotubes hybrid system on Ti implants.

assess the antibacterial ability of the modified Ti samples obtained above. They were cultured in Luria-Bertani (LB) medium. Briefly, different Ti samples were first treated under ultraviolet light (UV, λ = 254 nm) for 30 min with pure Ti served as control. Then 350 μL of diluted bacterial suspension (10^7 CFU/mL) was added into each well to immerse samples. The mixed solution was then incubated at 37 °C in a shaker incubator for 12 and 24 h for *E. coli* and *S. aureus*, respectively. The antibacterial activity against the early adherence of *E. coli* and *S. aureus* was first evaluated by SEM (SEM, JSM6510LV) and then quantified by measuring optical density (OD) at 600 nm with a microplate reader (SpectraMax i3, Molecular Devices).

2.5. Biocompatibility studies

Mouse calvarial cells (MC3T3-E1) were cultured with α-MEM (HyClone) medium containing 1% penicillin-streptomycin solution (HyClone) and 10% fetal bovine serum (FBS), followed by incubation in an atmosphere of 5% CO_2 incubator at 37 °C. The culture medium was changed every three days. The same culture conditions were used in all the experiments.

To evaluate osteoblast viability, the MTT assay was utilized. Ti samples with different hybrid coatings were incubated in 48-well plate with pure Ti samples served as control. Briefly, samples with MC3T3-E1 cells were cultured for 7 and 14 days in 48-well plates. The culture medium was changed every three days. After removal medium, 300 μL of the MTT solution (5 mg/mL in PBS) was added to each well, and the cells were additionally incubated for 4 h at 37 °C. 300 μL of dimethyl sulfoxide (DMSO) was then added to each well, followed by shaking at a shaking table for 10 min. The absorbance was measured at 570 nm using a microplate reader (SpectraMax i3, Molecular Devices). The percentage of cell viability was determined from the absorbance readings and calculated by dividing the values of the samples to that of the control.

To determine the osteogenic differentiation property of Ti samples with different hybrid nanostructures, the ALP assay was utilized. The same method mentioned above was used for the cell culture with samples and pure Ti as control for a period of 7 and 14 days in 48-well plates. After the culture period, the medium was removed. 500 μL/well of diluted Triton X-100 was aliquoted onto the surface of samples and then incubated at 37 °C for 60 min to lyse the cells. 30 μL of the cell lytic solution was mixed with ALP standard solution and then incubated at 37 °C for 30 min, followed by measurement of absorbance at 520 nm.

In order to evaluate the influence of samples on cells at early stage, SEM and live/dead staining method were utilized. Samples were first incubated with MC3T3-E1 cells at 37 °C for 8 h. For SEM imaging, cells were fixed onto the surface with 2.5% glutaraldehyde solution and then dehydrated sequentially in gradient ethanol solutions (30, 50, 70, 90, and 100 v/v%) for 15 min. For the live/dead

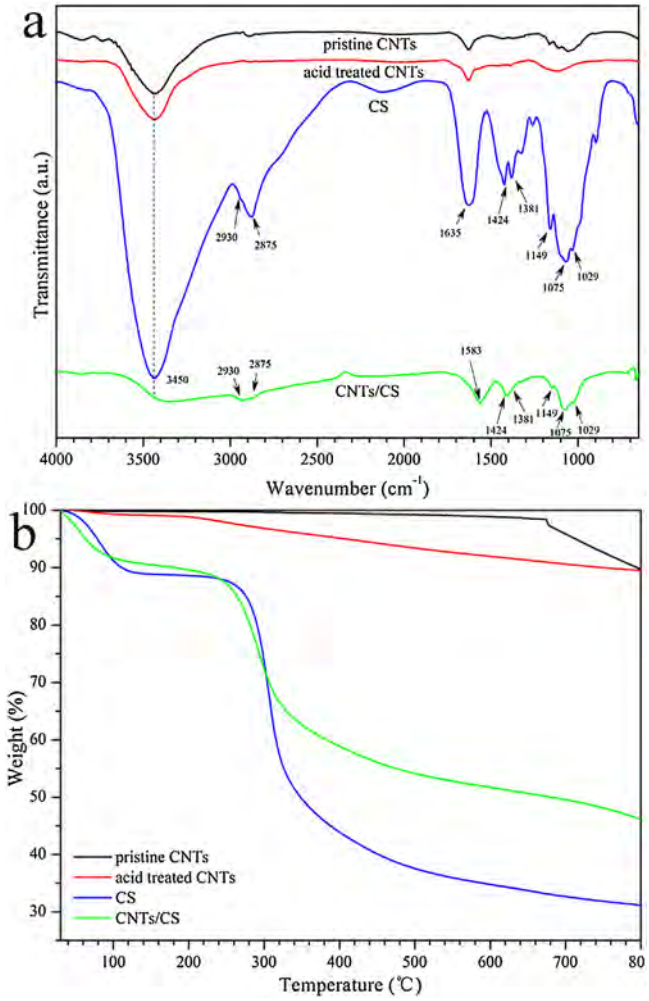

Fig. 1. (a) FT-IR spectra of pristine CNTs, acid treated CNTs, CS and CNTs/CS scraped from samples. (b) TGA curves of pristine CNTs, acid treated CNTs, CS and CNTs/CS scraped from samples.

staining, samples were first stained by propidium iodide (PI) for 20 min and then washed by PBS solution three times. Subsequently, acridine orange (AO) staining was proceeded in the same way. The live/dead staining was examined by the inverted fluorescence microscope (Olympus, IX73).

3. Results and discussion

3.1. Surface characteristics

The FTIR spectra of pristine CNTs, acid treated CNTs, CS and CNTs/CS scraped from the EDP samples indicates the presence of peaks associated with both CNTs and chitosan. As shown in Fig. 1a, the spectra of CNTs and acid treated CNTs show no significant difference. The peaks at 3450 cm^{-1} are ascribed to the stretching vibration of —OH superimposed on —NH stretching band and broadened after combined with chitosan. The spectrum of CNTs/CS contains characteristic peaks of all the raw material like those of chitosan and acid treated CNTs, confirming that chitosan has been successfully grafted to CNTs. Peaks at 2930 cm^{-1} and 2875 cm^{-1} are attributed to —CH_2 stretching vibration; the one at 1635 cm^{-1} is attributed to —NH_2 stretching vibration while the two peaks at 1381 and 1424 cm^{-1} are attributed to C—H bending vibration. Another two peaks located at 1070 and 1033 cm^{-1} are associated with the C—O—C and C—N stretching vibration mode, respectively. Additionally, a new absorption peak at 1586 cm^{-1} indicates an overlap of the amide band and the amino group of the chitosan which is in agreement with literatures [43–45], confirming the successful modification of the hybrid composed of CS and CNTs on Ti surfaces.

The thermal degradation of CNTs/CS is further confirmed by TGA. As shown in Fig. 1b, the total weight loss of pristine CNTs and acid treated CNTs is about 10%, a significant weight loss occurs at about 670 °C, which should be caused by the burning of CNTs. For CS and CNTs/CS scraped from the EDP samples, slightly weight loss before 150 °C are caused by the evaporation of residual solvent and water. Due to the burning of CS, a significant weight loss can be observed beginning at about 250 °C. The thermal degradation of CS ends at about 600 °C. The weight loss of CNTs/CS calculated between 250 °C and 600 °C is about 35%. These results suggested that CNTs were coated onto the surface of Ti.

XPS is utilized to analyze the chemical compositions of the hybrid nanostructures. As indicated by Fig. 2a, the elements including carbon (C), oxygen (O), nitrogen (N), titanium (Ti) and Zinc (Zn) are confirmed by the XPS survey scan ranging from 0 to 1200 eV. The detailed information of C1s, N1s, O1s, Ti2p, and Zn2p is shown by XPS narrow scan spectra. As shown in Fig. 2b, the C1s peak of AHT shows a binding energy at 285.5 eV, which is possibly soriginated from surface contamination (CO_2 and organics in air). After modified with CNTs/CS, two dominant peaks at 284.4 eV and 286.5 eV emerge, and the former can be assigned to graphitic C from CNTs [46] while the latter is contributed to C—O band from CS [47], respectively. However, after the deposition of ZnO by ALD, the signals become weaker gradually as the number of deposition cycle increases. After 300 cycles, the thickness of ZnO film deposited onto CNTs/CS is about 10 nm (shown in Fig. 3), the signals assigned to both C—O and C—C become very weak (shown by the fitting curve in Fig. S1). It is believed that the thicker ZnO film blocks the signals from CNTs and CS. As shown in Fig. 2**c**, O1s spectrum detected from AHT exhibits a widen curve, and the fitting curve displays two peaks at 530.4 and 532.3 eV (shown in Fig. S2). The former is assigned to O–Metal from titanates on the surface of AHT while the latter is due to the contamination. O1 s spectrum obtained from CNTs/CS modified AHT sample has no O–Metal bond. The dominant is O—C band from CS, and the weak signal of O=C bond is caused by surface contaminations (shown in Fig. S3). The subsequently deposited ZnO films gradually blocked the signal of O—C band from CS and enhanced the signal of O—Metal bond from ZnO. After 300 cycles, O—C band shows very weak signal while the one of O—Metal bond at 530.4 eV becomes much stronger due to the thicker ZnO film (shown in Fig. S4). As shown in Fig. 2d, the nitrogen signal at a binding energy of 399.2 eV is corresponding to chitosan's amine groups, and decreases as the thickness of ALD-ZnO film increasing. As shown in Fig. 2e, the two peaks of Ti2p detected from AHT are located at 461 and 465 eV, related to typical titanium dioxides or titanates [48]. After modified by CNTs/CS/ZnO films, this signal was fully suppressed. These results demonstrated that CNTs had been successfully modified with CS. The two peaks of Zn2p at 1022.7 and 1045.5 eV assigned to ZnO shown in Fig. 2**f** become stronger as the increase of ALD deposition cycles, indicating the increased thickness of deposition film. The Zn content increases from 3.25% of CNTs/CS-ZnO(30) to 37.45% of CNTs/CS-ZnO(300). The similar spectra of C1s, O1s and N1s spectra detected from CNTs/CS-ZnO(30) and CNTs/CS-ZnO(100) indicate that the low temperature ALD process cannot change the chemical composition of CNTs/CS composites.

To investigate the morphology of CNTs before and after modification, TEM is applied. Fig. 3a shows CNTs after acid treatment, it can be seen that the wall of the as-received CNTs is smooth. After modification with CS and EDP on Ti surface, uneven coating on CNTs can be clearly observed in Fig. 3b (as indicated by the red arrows), further demonstrating that CNTs have been successfully modified with CS. The ALD-ZnO on CNTs at 80 °C is shown in Fig. 3c, d, and e. After 30 cycles, a uniform and smooth thin film less than 2 nm can be observed (Fig. 3c) on CNTs. The deposition with 100 cycles can produce a thin film with a thickness of about 5 nm (Fig. 3d). Once the numbers of deposition cycles are increased to 300, the corresponding thickness of ZnO films is increased to 10 nm (Fig. 3e). The selected area electron diffraction (SAED) patterns of CNTs/CS, CNTs/CS-ZnO(30), CNTs/CS-ZnO(100) and CNTs/CS-ZnO(300) are shown in the insert images, respectively (Fig. 3a–e). The SAED pattern reveals the polycrystalline nature of CNTs/CS-ZnO samples, confirming that ZnO films were successfully deposited onto the surface of samples.

The surface morphologies of the samples after alkali-heat-treatment, EDP coated with CNTs/CS, ALD coated with 30, 100, 300 cycles of ZnO have been characterized by FE-SEM. As shown in Fig. 4a, after alkali-heat-treatment, the surface of Ti specimens shows a rough multilayer nanoscale mesh crosslinking structure with pores diameter of about 100–200 nm, which provides a rough and high surface area. Fig. 4b shows the morphology of samples coated with CNTs/CS. CNTs are entangled on the surface and wrapped in CS, forming a network with pore structure. The distribution of CNTs is uniform which may be due to the electrically charged nature of chitosan. After ZnO deposition, the wall thickness of CNTs increases and the surface becomes rougher as the deposition cycle numbers increased. The wall with 30 cycles ALD-ZnO on CNT is smooth, compared to those with 100 and 300 cycles. After 100 and 300 cycles of ALD-ZnO deposition, numerous tiny particles can be seen on CNTs and CS (shown in FE-SEM and high magnification images inserted in Fig. 4c–e).

3.2. Antibacterial tests

As shown in Fig. 5a, compared to those samples without ZnO, ZnO modified samples have higher antibacterial ratio. Moreover, samples with CNTs/CS-ZnO exhibited a better antibacterial properties than AHT-ZnO ones. The antibacterial ratio against *E. coli* of AHT-ZnO(30) and CNTs/CS-ZnO(30) is about 35% and 43%, respectively. Similarly, the antibacterial ratio against *S. aureus* of AHT-ZnO(30) is smaller than CNTs/CS-ZnO(30). Samples with CNTs/CS exhibited better antibacterial properties than AHT ones. However, when the cycling numbers of ALD-ZnO increase to 100

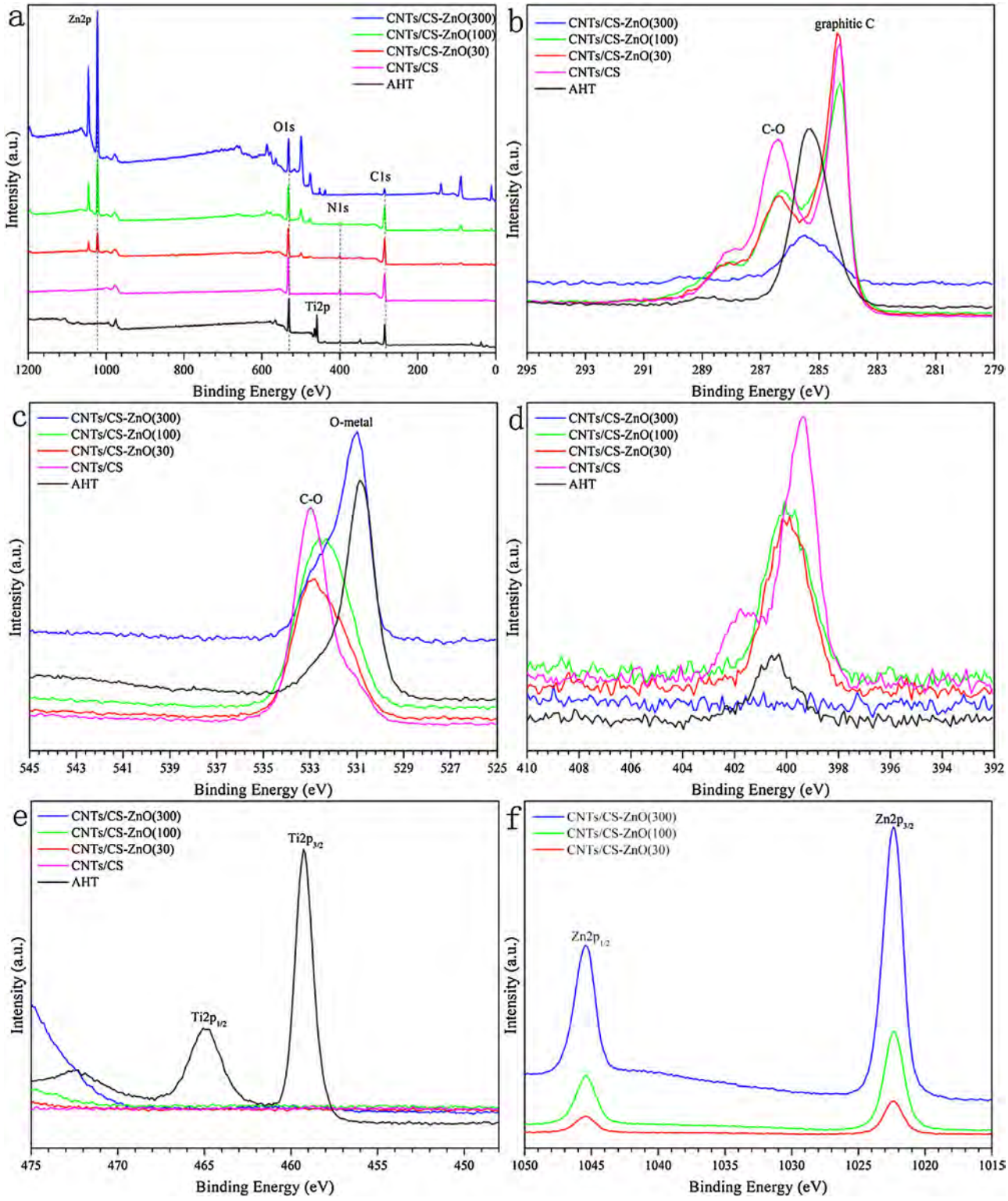

Fig. 2. XPS spectra of AHT, CNTs/CS, CNTs/CS-ZnO(30), CNTs/CS-ZnO(100) and CNTs/CS-ZnO(300). (a) Survey scan ranges from 0 to 1200 eV. (b) The C1s region, (c) O1s region, (d) N1 s region, (e) Ti2p region, (f) Zn2p region.

and 300, the antibacterial ratio against *E. coli* and *S. aureus* increased to a steady value of over 73% and 98%, respectively.

The morphology and membrane integrity of bacteria can be evaluated by SEM. As shown in Fig. 5b, *E. coli* on pure Ti has intact walls. After modified with CNTs/CS and ZnO with different cycles, bacteria corrugated with distorted shapes and incomplete membranes (red arrows) are shown in Fig. 5b. Similarly, the typical morphology of *S. aureus* with a spherical shape and smooth surface can be observed on pure Ti, shown in Fig. 5b. Although some of *S. aureus* maintains the membrane integrity after CNTs/CS-ZnO modification, bacteria with corrugated membranes (red arrows) and irregular shape can be observed in Fig. 5b.

As shown in Fig. S5, the total Zn contents in CNTs/CS-ZnO(30), CNTs/CS-ZnO(100) and CNTs/CS-ZnO(300) are 7.3, 16.4

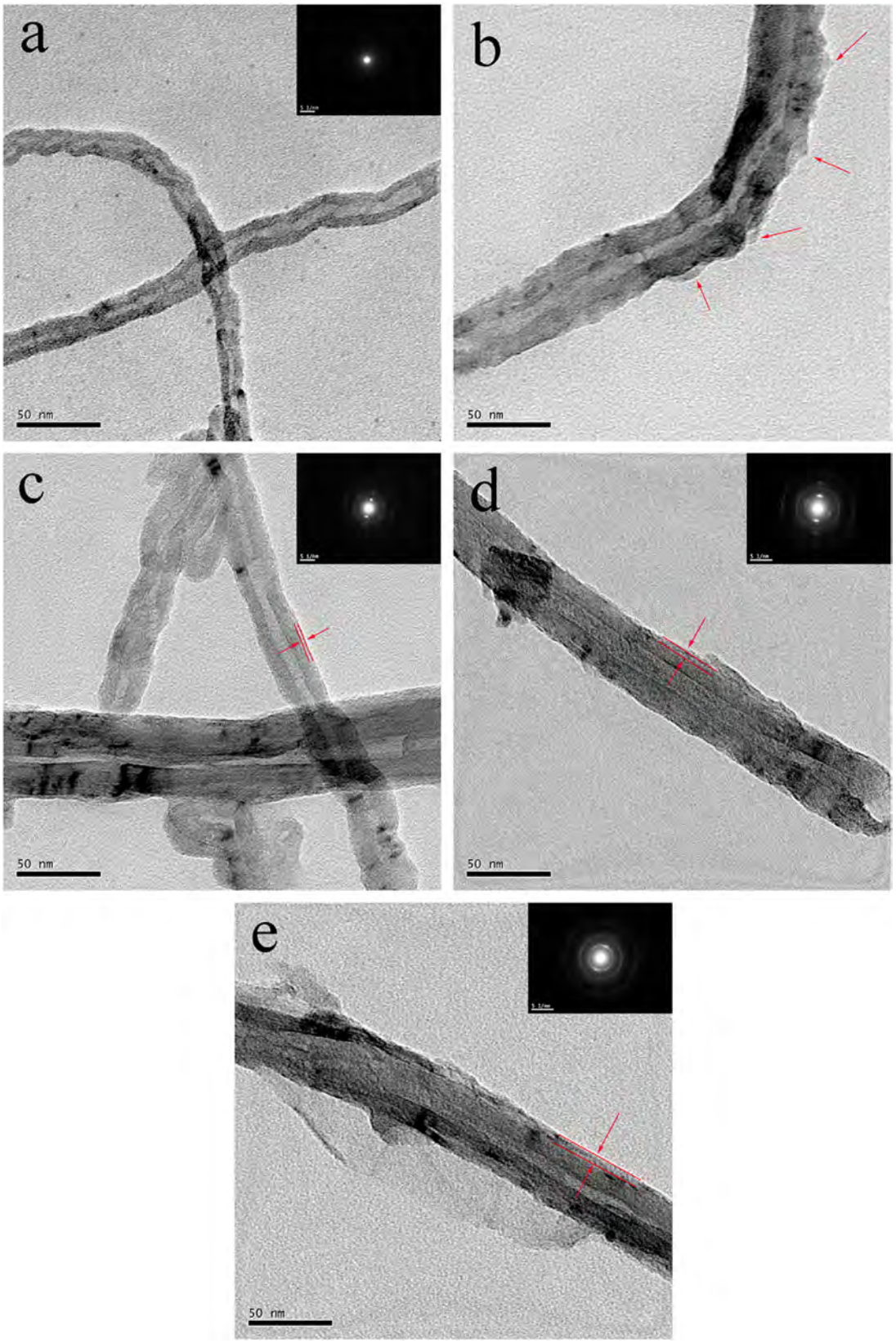

Fig. 3. Representative TEM images and the corresponding selected area electron diffraction (SAED) patterns of acid treated (a) CNTs, (b) CNTs/CS scraped from samples, (c) CNTs/CS-ZnO(30) scraped from samples, (d) CNTs/CS-ZnO(100) scraped from samples and (e) CNTs/CS-ZnO(300) scraped from samples, scale bar = 50 nm.

and 95.7 μg, respectively. It has been reported that Zinc ion released from ZnO can increase the generation time of the organisms [49] and changing the fluidity of the membrane [50] by combining with cell membranes of bacteria, which can be schematically illustrated by Scheme 1. This lead to the destruction of protein structures, the inactivation and death of cells [51]. It has been reported that the

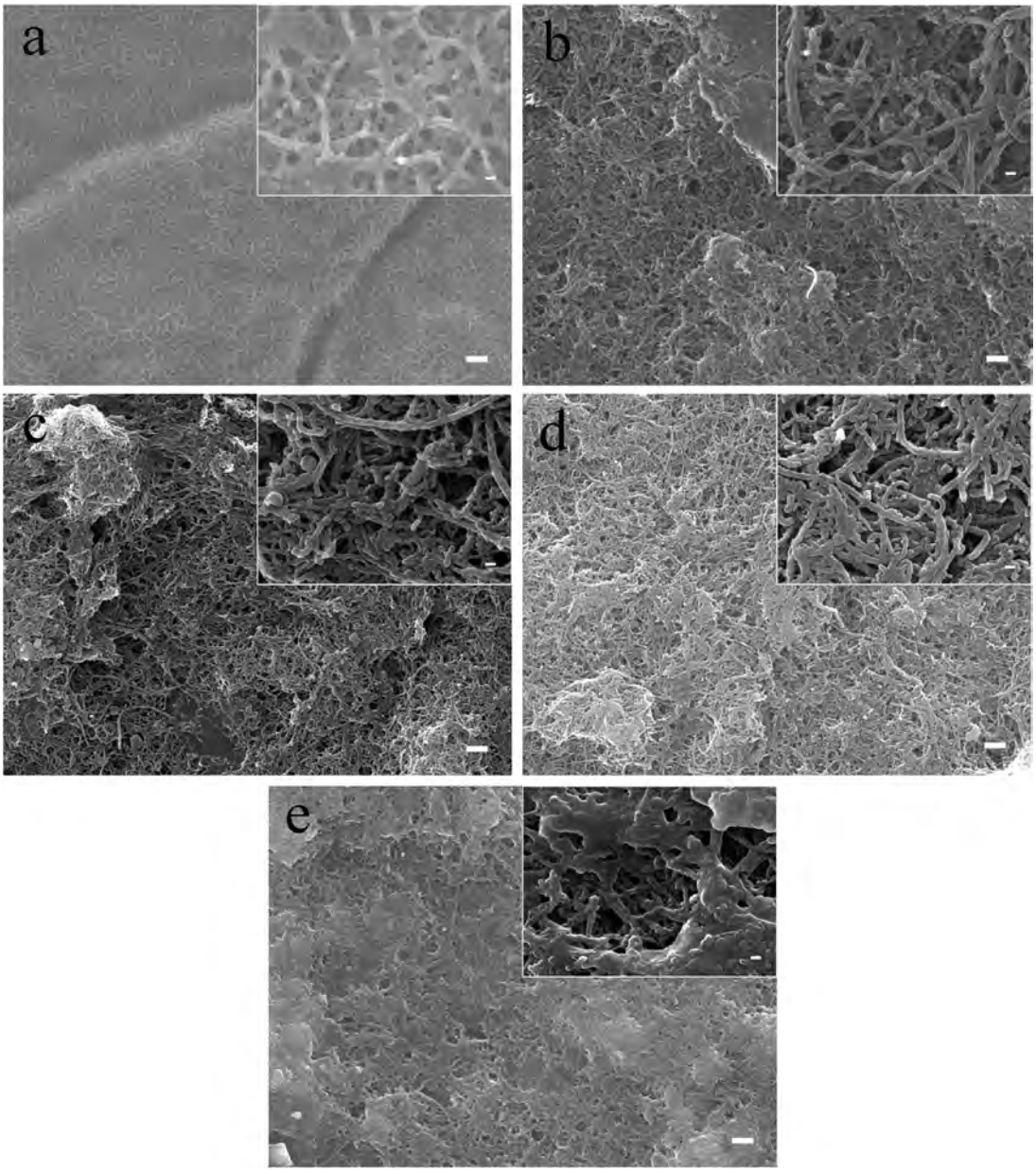

Fig. 4. FE-SEM images of (a) AHT, (b) CNTs/CS, (c) CNTs/CS-ZnO(30), (d) CNTs/CS-ZnO(100), (e) CNTs/CS-ZnO(300). Insets are high magnification FE-SEM images. The scale bar is 1 μm and the scale bar of insets is 100 nm.

ROS generation due to the photocatalysis of ZnO also has a great impact on antibacterial properties [33]. When light is absorbed, the negatively charged electrons and positively charged holes are created [52]. These electron-hole pairs can generate ROS by reacting with oxygen and hydroxyl absorbed on the surface of substrates and water. The increased level of ROS causes an enhanced oxidative stress and can inhibit the proliferation of bacterial cells or kill them by reacting with organic compounds in microorganisms [32,52]. After 100 or 300 cycles of ZnO deposited on samples, adequate content of ZnO plays a guiding role of the antibacterial mechanism. Several researches have proved that CNTs can effectively inhibit the recombination of electron-hole pairs and thus enhance the photocatalytic activity of ZnO [53–55]. The result mentioned above indicated that CNTs/CS could enhance the antibacterial activity especially with a less content of ZnO. And the content of Zn and thus Zn^{2+} released from samples are tunable by changing the cycling number of ALD.

3.3. Evaluation of cytocompatibility

As shown in Fig. 6a, samples with CNTs/CS and CNTs/CS-ZnO(30) exhibit no significant inhibition of cell proliferation compared to pure Ti as control. However, with the content of ZnO increasing, CNTs/CS-ZnO reduced proliferation over a same period of time, especially for samples with 300 cycles of ZnO. Although ZnO coated samples inhibit the cell proliferation with the general trend of cell viability ratio decrease with ALD-ZnO cycles increase, the cell viability increases after modified with CNTs/CS compared to AHT samples with same content of ZnO.

Alkaline phosphatase activity (ALP) is an important marker for osteogenic differentiation. As Fig. 6b shows, after 7 days of cell culture, the cells already produce a certain amount of ALP with a trend of CNTs/CS-ZnO(300) > CNTs/CS-ZnO(100) > CNTs/CS-ZnO(30). After 14 days, a similar trend is also observed. Samples with CNTs/CS produce more ALP than AHT with same content of

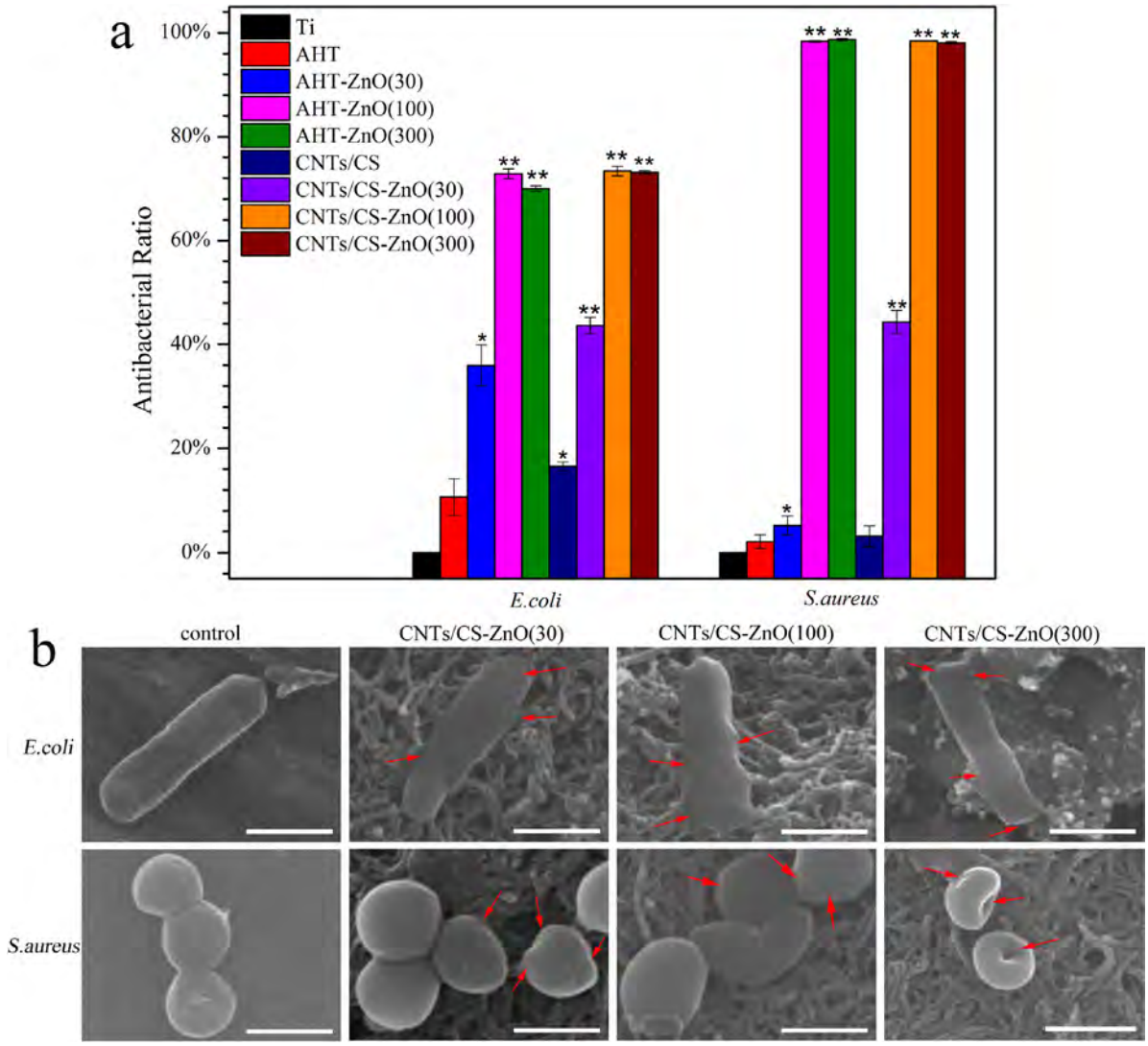

Fig. 5. Antibacterial activity of different samples against *E. coli* and *S. aureus*. (a) Antibacterial ratio of Ti, AHT, CNTs/CS, CNTs/CS-ZnO(30), CNTs/CS-ZnO(100) and CNTs/CS-ZnO(300) against *E. coli* and *S. aureus*. (b) SEM images of the attachment of *E. coli* and *S. aureus* cells to untreated Ti surface, CNTs/CS-ZnO(30), CNTs/CS-ZnO(100) and CNTs/CS-ZnO(300) after incubation at 37 °C for 12 and 24 h, respectively. The scale bar is 1 μm. *P < 0.05 and **P < 0.01 versus the Ti group.

ZnO over a same period of time, indicating that CNTs/CS composites can enhance synthesis of ALP. These results confirmed that not only ZnO significantly increased the ALP activity but also CNTs/CS coating played an important role in promoting osteogenic differentiation.

To further understand the impact of nanostructures on cell, SEM is utilized to observe the surface of cells incubated on samples. As shown in Fig. 6c, MC3T3-E1 cells could be observed after 8 h of cell culture on samples with different modifications. Cells grow flat on AHT. Similarly, cells spread on CNTs/CS with long threadlike cytoplasmic anchored to nanotube bundles. However, cell bodies are spherical when cultured on nanostructures with different content of ZnO. As shown in Fig. 6c, thin pseudopods with prolonged threadlike cytoplasmic can be observed on CNTs/CS-ZnO(30). Similarly, round cell bodies with developed pseudopods can be observed on CNTs/CS-ZnO(100) and CNTs/CS-ZnO(300). These cell morphologies indicate the fully differentiated osteoblasts embedded in the bone matrix [17]. Although it has been reported that overdosed Zn can introduce cytotoxicity since the cytotoxicity of Zn is dose dependent [56]. The cytotoxicity of ZnO nanostructures can be minimized by cooperating with CNTs/CS composites and controlling the content of ZnO by changing the cycling number of ALD. Compared to Ti, CNTs/CS-ZnO samples provided rougher surfaces (shown in Table S1), which have been reported to be good for osteogenic differentiation and the formation of bone matrix [57,58]. Compared to Ti, CNTs/CS-ZnO samples provided It has been reported that CNTs coated Ti could exhibit strong cell adhesions [59]. Researchers have reported that cells attach to material surface through specific protein [60], rather than directly attach to the surface [60–64]. Different contents of ZnO deposited on CNTs/CS samples with hydrophobic surfaces (Fig. S6) may present less amounts of cells but be conducive for protein adsorption [60]. At the early stage of cell adhesion and proliferation, few cells are dead on CNTs/CS-ZnO samples (Shown in Fig. S7). Combined with the results mentioned above, appropriate contents of ZnO with CNTs/CS exhibit no significant cytotoxicity on cells. However, increased content of ZnO may inhibit cell proliferation compared to samples without ZnO in same periods of time. Many studies have documented that Zn can regulate bone formation at a cellular level. As an essential trace element, Zn can not only induce the expression of osteoblast differentiation genes, including osteopontin, runt-related transcription factor 2 and bone sialoprotein [65] but also stimulate protein tyrosine phosphatase activity [66]. Results mentioned above indicate that ZnO promotes osteogenic

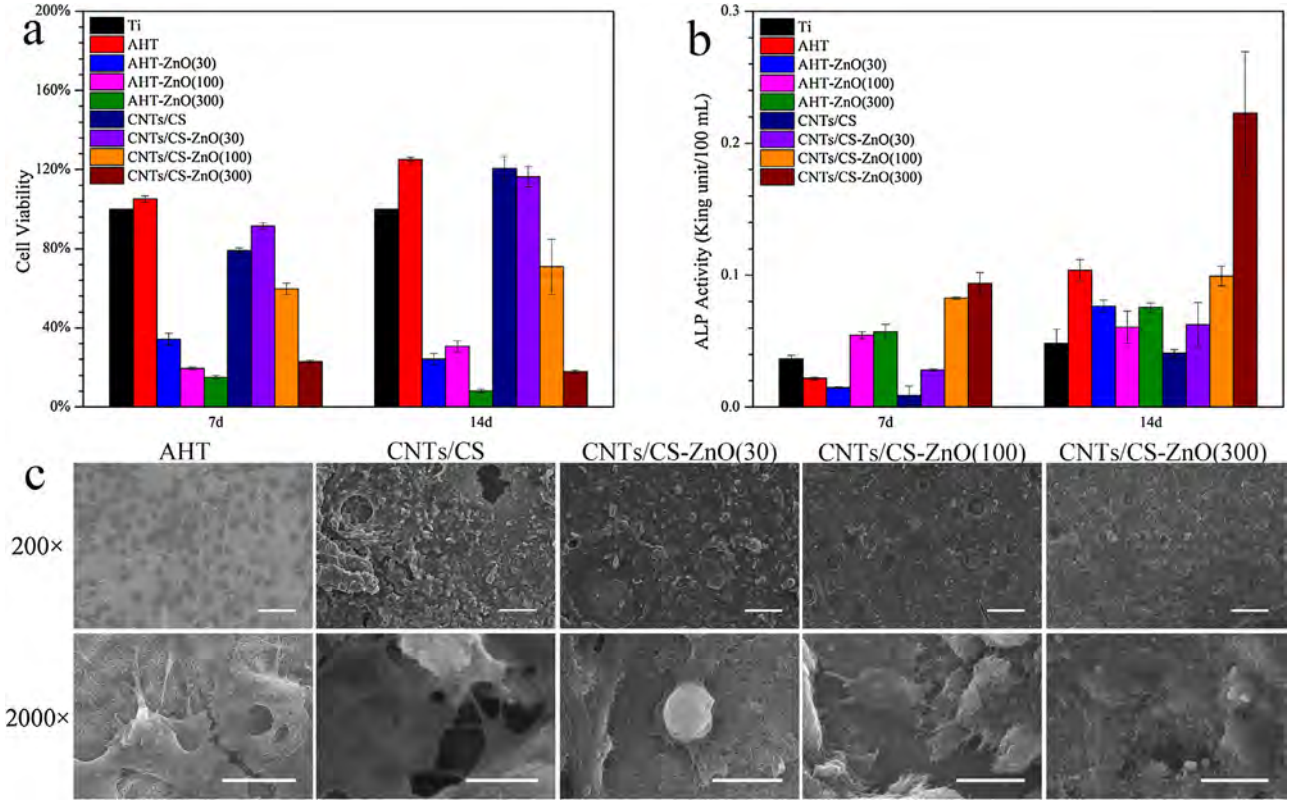

Fig. 6. (a) Cell viability of MC3T3-E1 cells cultured on Ti, AHT, CNTs/CS, CNTs/CS-ZnO(30), CNTs/CS-ZnO(100) and CNTs/CS-ZnO(300) for 7 and 14 days. (b) ALP activity of MC3T3-E1 cells cultured on Ti, AHT, CNTs/CS, CNTs/CS-ZnO(30), CNTs/CS-ZnO(100) and CNTs/CS-ZnO(300) for 7 and 14 days. (c) SEM images of cells on samples surfaces after incubated for 8 h. The scale bar is 100 μm for low magnification and 10 μm for high magnification, respectively.

differentiation and produces more ALP in a same period of time with more ZnO.

These results indicate that the increasing content of zinc can inhibit the cell proliferation but promote osteogenic differentiation. Since the content of ZnO is determined by the tunable cycling number of ALD-ZnO process, our results show a facile way to regular cell behavior by changing the content of ZnO deposited on CNTs/CS.

4. Conclusions

1 D nanostructures of ZnO on CNTs/CS modified Ti are prepared by using ALD. These novel hybrid nanostructures have been comprehensive characterized as well as evaluated for their potential application as an antibacterial material used as Ti implants. The thickness of ZnO coated and the content of Zn can be controlled by adjusting cycling numbers. The ALD-ZnO modified samples show good antibacterial effects and enhanced osteogenic differentiation ability by increasing the photocatalicity activity of ZnO through inhibiting the recombination of electron-hole pairs in ZnO by CNTs. Our results suggest that the antibacterial hybrid nanostructures on Ti implants can also regulate the proliferation and osteogenic differentiation of osteoblasts by controlling the cycling numbers of ALD-ZnO.

Acknowledgements

This work is jointly supported by Special Prophase Program for Key Basic Research of the Ministry of Science and Technology of China (973 Program) No. 2014CB660809, and the National Natural Science Foundation of China Nos. 51422102, and 81271715.

Appendix A. Supplementary data

Supplementary data associated with this article can be found, in the online version, at http://dx.doi.org/10.1016/j.apsusc.2016.12.158.

References

[1] J.A. Helsen, H.J. Breme, Metals as Biomaterials, Chichester, New York, 1998, pp. 30–40.
[2] K.G. Neoh, X. Hu, D. Zheng, E.T. Kang, Balancing osteoblast functions and bacterial adhesion on functionalized titanium surfaces, Biomaterials 33 (2012) 2813–2822.
[3] M. Li, X. Liu, Z. Xu, K.W.K. Yeung, S. Wu, Dopamine modified organic-inorganic hybrid coating for antimicrobial and osteogenesis, ACS Appl. Mater. Interfaces 8 (49) (2016) 33972–33981.
[4] R.O. Darouiche, Treatment of infections associated with surgical implants, N. Engl. J. Med. 350 (2004) 1422–1429.
[5] X. Liu, M. Li, Y. Zhu, K.W.K. Yeung, P.K. Chu, S. Wu, The modulation of stem cell behaviors by functionalized nanoceramic coatings on Ti-based implants, Bioact. Mater. 1 (2016) 65–76.
[6] S. Wu, X. Liu, K.W.K. Yeung, C. Liu, X. Yang, Biomimetic porous scaffolds for bone tissue engineering, Mater. Sci. Eng. R. 80 (2014) 1–36.
[7] Z. Xu, L. Man, L. Xia, X. Liu, M. Fei, S. Wu, K.W.K. Yeung, Y. Han, P.K. Chu, Antibacterial activity of silver doped titanate nanowires on Ti implants, ACS Appl. Mater. Interfaces 8 (2016) 16584–16594.
[8] T. Zhou, Y. Zhu, X. Li, X. Liu, K.W.K. Yeung, S. Wu, X. Wang, Z. Cui, X. Yang, P.K. Chu, Surface functionalization of biomaterials by radical polymerization, Prog. Mater. Sci. 83 (2016) 191–235.
[9] M. Cinke, J. Li, B. Chen, A. Cassell, L. Delzeit, J. Han, M. Meyyappan, Pore structure of raw and purified HiPco single-walled carbon nanotubes, Chem. Phys. Lett. 365 (2012) 69–74.
[10] M. Terrones, Science and technology of the twenty-first century: synthesis, properties, and applications of carbon nanotubes, Annu. Rev. Mater. Res. 33 (1) (2003) 419–501.
[11] X. Wei, M.S. Wang, Y. Bando, D. Golberg, Thermal stability of carbon nanotubes probed by anchored tungsten nanoparticles, Sci. Technol. Adv. Mater. 12 (2011) 044605–044611.

[12] S. Kang, M. Pinault, L.D. Pfefferle, M. Elimelech, Single-walled carbon nanotubes exhibit strong antimicrobial activity, Langmuir 23 (2007) 8670–8673.
[13] L.R. Arias, L. Yang, Inactivation of bacterial pathogens by carbon nanotubes in suspensions, Langmuir 25 (2009) 3003–3012.
[14] D. Nepal, S. Balasubramanian, A.L. Simonian, V.A. Davis, Strong antimicrobial coatings: single-walled carbon nanotubes armored with biopolymers, Nano Lett. 8 (2008) 1896–1901.
[15] T. Akasaka, F. Watari, Capture of bacteria by flexible carbon nanotubes, Acta Biomater. 5 (2009) 607–612.
[16] S. Kang, M. Herzberg, D.F. Rodrigues, M. Elimelech, Antibacterial effects of carbon nanotubes: size does matter!, Langmuir 24 (2008) 6409–6413.
[17] K. Rajavel, R. Gomathi, S. Manian, In vitro bacterial cytotoxicity of CNTs: reactive oxygen species mediate cell damage edges over direct physical puncturing, Langmuir 30 (2013) 592–601.
[18] J.E. Park, I.S. Park, M.P. Neupane, T.S. Bae, M.H. Lee, Effects of a carbon nanotube-collagen coating on a titanium surface on osteoblasts growth, Appl. Surf. Sci. 292 (2014) 828–836.
[19] R.L. Price, M.C. Waid, K.M. Haberstroh, T.J. Webster, Selective bone cell adhesion on formulations containing carbon nanofibers, Biomaterials 24 (2003) 1877–1887.
[20] K.L. Elias, R.L. Price, T.J. Webster, Enhanced functions of osteoblasts on nanometer diameter carbon fibers, Biomaterials 23 (2002) 3279–3287.
[21] M.D. Nicola, D.M. Gattia, S. Bellucci, G.D. Bellis, F. Micciulla, R. Pastore, A. Tiberia, C. Cerella, M. D'Alessio, M.V. Antisari, R. Marazzi, E. Traversa, A. Magrini, A. Bergamaschi, L. Ghibelli, Effect of different carbon nanotubes on cell viability and proliferation, J. Phys.-Condens. Mater. 19 (2007) 395013.
[22] S.J. Choi, J.M. Oh, J.H. Choy, Toxicological effects of inorganic nanoparticles on human lung cancer A549 cells, J. Inorg. Biochem. 103 (2009) 463–471.
[23] E. Herzog, H.J. Byrne, M. Davoren, A. Casey, A. Duschl, G.J. Oostingh, Dispersion medium modulates oxidative stress response of human lung epithelial cells upon exposure to carbon nanomaterials samples, Toxicol. Appl. Pharm. 236 (2009) 276–281.
[24] D. Cui, F. Tian, C.S. Ozkan, M. Wang, H. Gao, Effect of single wall carbon nanotubes on human HEK293 cells, Toxicol. Lett. 155 (2005) 73–85.
[25] P. Ravichandran, A. Periyakaruppan, B. Sadanandan, V. Ramesh, J.C. Hall, O. Jejelowo, G.T. Ramesh, Induction of apoptosis in rat lung epithelial cells by multiwalled carbon nanotubes, J. Biochem. Mol. Toxicol. 23 (2009) 333–344.
[26] A.D. Martino, M. Sittinger, M.V. Risbud, Chitosan: a versatile biopolymer for orthopaedic tissue-engineering, Biomaterials 26 (2005) 5983–5990.
[27] R.A.A. Muzzarelli, Chitosan composites with inorganics morphogenetic proteins and stem cells, for bone regeneration, Carbohydr. Polym. 83 (2011) 1433–1445.
[28] F. Pishbin, V. Mouriño, J.B. Gilchrist, D.W. Mccomb, S. Kreppel, V. Salih, M.P. Ryan, Single-step electrochemical deposition of antimicrobial orthopaedic coatings based on a bioactive glass/chitosan/nano-silver composite system, Acta Biomater. 9 (2013) 7469–7479.
[29] F. Pishbin, V. Mouriño, S. Flor, S. Kreppel, V. Salih, M.P. Ryan, A.R. Boccaccini, Electrophoretic deposition of gentamicin-loaded bioactive glass/chitosan composite coatings for orthopaedic implants, ACS Appl. Mater. Interfaces 6 (2014) 8796–8806.
[30] Z. Zhong, J. Qin, J. Ma, Electrophoretic deposition of biomimetic zinc substituted hydroxyapatite coatings with chitosan and carbon nanotubes on titanium, Ceram. Int. 41 (2015) 8878–8884.
[31] O.M. Goudouri, E. Kontonasaki, U. Lohbauer, A.R. Boccaccini, Antibacterial properties of metal and metalloid ions in chronic periodontitis and peri-implantitis therapy, Acta Biomater. 10 (2014) 821–854.
[32] P. Zhu, Z. Weng, X. Li, X. Liu, S. Wu, K.W.K. Yeung, X. Wang, Z. Cui, J. Yang, P.K. Chu, Biomedical applications of functionalized ZnO nanomaterials: from biosensors to bioimaging, Adv. Mater. Interfaces 3 (2016) 201500494.
[33] G. Applerot, A. Lipovsky, R. Dror, N. Perkas, Y. Nitzan, R. Lubart, A. Gedanken, Enhanced antibacterial activity of nanocrystalline ZnO due to increased ROS-mediated cell injury, Adv. Funct. Mater. 19 (2009) 842–852.
[34] A. Kahru, H.C. Dubourguier, I. Blinova, A. Ivask, K. Kasemets, Biotests and biosensors for ecotoxicology of metal oxide nanoparticles: a minireview, Sensors 8 (2008) 5153–5170.
[35] R.S. Macdonald, The role of zinc in growth and cell proliferation, J. Nutr. 130 (2000) 1500S–1508S.
[36] S. Kwun, Y.E. Cho, R.A.R. Lomeda, H.I. Shin, J.Y. Choi, Y.H. Kang, J.H. Beattie, Zinc deficiency suppresses matrix mineralization and retards osteogenesis transiently with catch-up possibly through Runx 2 modulation, Bone 46 (2010) 732–741.
[37] T. Suntola, J. Antson, Method for producing compound thin films (1977) US. 4058430.
[38] S.M. George, Atomic layer deposition: an overview, Chem. Rev. 110 (2010) 111–131.
[39] X. Meng, M.N. Banis, D. Geng, X. Li, Y. Zhang, R. Li, H.A. Rachid, Controllable atomic layer deposition of one-dimensional nanotubular TiO_2, Apply. Surf. Sci. 266 (2013) 132–140.
[40] R. Narayanan, T.Y. Kwon, K.H. Kim, TiO_2 nanotubes from stirred glycerol/NH_4F electrolyte: roughness, wetting behavior and adhesion for implant applications, Mater. Chem. Phys. 117 (2009) 460–464.
[41] J. Liu, A.G. Rinzler, H.J. Dai, J.H. Hafner, R.K. Bradley, P.J. Boul, A. Lu, T. Iverson, K. Shelimov, C.B. Huffman, F. Rodriguez-Macias, Y.S. Shon, T.R. Lee, D.T. Colbert, R.E. Smalley, Fullerene pipes, Science 280 (1998) 1253–1256.
[42] C.V. Eiff, G. Peters, C. Heilmann, Pathogenesis of infections due to coagulase-negative staphylococci, Lancet Infect. Dis. 2 (2002) 677–685.
[43] G. Ke, W. Guan, C. Tang, W. Guan, D. Zeng, F. Deng, Covalent functionalization of multiwalled carbon nanotubes with a low molecular weight chitosan, Biomacromolecules 8 (2007) 322–326.
[44] Z. Wu, W. Feng, Y. Feng, Q. Liu, X. Xu, T. Sekino, A. Fujii, M. Ozaki, Preparation and characterization of chitosan-grafted multiwalled carbon nanotubes and their electrochemical properties, Carbon 45 (2007) 1212–1218.
[45] F. Yao, W. Chen, H. Wang, H. Liu, K. Yao, P. Sun, H. Lin, A study on cytocompatible poly(chitosan-g-l-lactic acid), Polymer 44 (2003) 6435–6441.
[46] X. Zhang, J. Ji, X. Zhang, B. Yang, M. Liu, W. Liu, L. Tao, Y. Chen, Y. Wei, Mussel inspired modification of carbon nanotubes using raft derived stimuli-responsive polymers, Rsc. Adv. 3 (2013) 21817–21823.
[47] Y.M. Nikolenko, V.G. Kuryavyi, I.V. Sheveleva, L.A. Zemskova, V.I. Sergienko, Atomic force microscopy and X-ray photoelectron spectroscopy study of chitosan-carbon fiber materials, Inorg. Mater. 3 (2010) 221–225.
[48] S. Wu, C.Y. Chung, X. Liu, P.K. Chu, J.P.Y. Ho, C.L. Chu, Y.L. Chan, K.W.K. Yeung, W.W. Lu, K.M.C. Cheung, K.D.K. Luk, Pore formation mechanism and characterization of porous NiTi shape memory alloys synthesized by capsule-free hot isostatic pressing, Acta Mater. 55 (2007) 3437–3451.
[49] L.L. Radke, B.L. Hahn, D.K. Wagner, P.G. Sohnle, Effect of abscess fluid supernatants on the kinetics of candida albicans growth, Clin. Immunol. Immunopathol. 73 (1994) 344–349.
[50] T.A. Söderberg, B. Sunzel, S. Holm, T. Elmros, G. Hallmans, S. Sjöberg, Antibacterial effect of zinc oxide in vitro, Scand. J. Plast. Recons. 24 (1990) 193–197.
[51] K. Hirota, M. Sugimoto, M. Kato, K. Tsukagoshi, T. Tanigawa, H. Sugimoto, Preparation of zinc oxide ceramics with a sustainable antibacterial activity under dark conditions, Cream. Int. 36 (2010) 497–506.
[52] R. Wahab, A. Mishra, S.I. Yun, I.H. Hwang, J. Mussarat, A.A. Al-Khedhairy, Y.S. Kim, H.S. Shin, Fabrication, growth mechanism and antibacterial activity of ZnO micro-spheres prepared via solution process, Biomass Bioenergy 39 (2012) 227–236.
[53] T.A. Saleh, M.A. Gondal, Q.A. Drmosh, Z.H. Yamani, A. Al-Yamani, Enhancement in photocatalytic activity for acetaldehyde removal by embedding zno nano particles on multiwall carbon nanotubes, Chem. Eng. J. 166 (2011) 407–412.
[54] L.P. Zhu, G.H. Liao, W.Y. Huang, L.L. Ma, Y. Yang, Y. Yu, S.Y. Fu, Preparation, characterization and photocatalytic properties of ZnO-coated multi-walled carbon nanotubes, Mater. Sci. Eng. B 163 (2009) 194–198.
[55] M. Samadi, H.A. Shivaee, M. Zanetti, A. Pourjavadi, A. Moshfegh, Visible light photocatalytic activity of novel MWCNT-doped ZnO electrospun nanofibers, J. Mol. Catal. A-Chem. 359 (2012) 42–48.
[56] E. Saino, S. Grandi, E. Quartarone, V. Maliardi, D. Galli, N. Bloise, L. Fassina, M.G. De Angelis, P. Mustarelli, M. Imbriani, L. Visai, In vitro calcified matrix deposition by human osteoblasts onto a zinc-containing bioactive glass, Eur. Cells Mater. 21 (2011) 59–72.
[57] B. Yang, M. Uchida, H.M. Kim, X. Zhang, T. Kokubo, Preparation of bioactive titanium metal via anodic oxidation treatment, Biomaterials 25 (2004) 1003–1010.
[58] X. Zhu, J. Chen, L. Scheideler, T. Altebaeumer, J. Geisgerstorfer, D. Kern, Cellular reactions of osteoblasts to micron- and submicron-scale porous structures of titanium surfaces, Cells Tissues Organs 178 (2004) 13–22.
[59] S. Abe, K. Ishikawa, A. Hyono, H. Kobayashi, T. Kiba, T. Akasaka, M. Uo, Y. Yawaka, S.I. Sato, T. Yonezawa, F. Watari, Observation of a 3D network nano-structure of carbon nanotubes scaffold for cultivation, e-J. Surf. Sci. Nanotechnol. 5 (2011) 80–84.
[60] A.K. Patel, P. Trivedi, K. Balani, Carbon nanotube functionalization decreases osteogenic differentiation in aluminum oxide reinforced ultrahigh molecular weight polyethylene, ACS Biomater. Sci. Eng. 2 (2016) 1242–1256.
[61] J.L. Dewez, A. Doren, Y.J. Schneider, P.G. Rouxhet, Competitive adsorption of proteins: key of the relationship between substratum surface properties and adhesion of epithelial cells, Biomaterials 20 (1999) 547–559.
[62] Q. Yu, Y. Zhang, H. Chen, F. Zhou, Z. Wu, H. Huang, J.L. Brash, Protein adsorption and cell adhesion/detachment behavior on dual-responsive silicon surfaces modified with poly(N-isoproplylacrylamide)-block-polystyrene copolymer, Langmuir 26 (2010) 8582–8588.
[63] Y. Xu, M. Takai, K. Ishihara, Protein adsorption and cell adhesion on cationic, neutral, and anionic 2-methacryloyloxyethyl phosphorylcholine copolymer surfaces, Biomaterials 30 (2009) 4930–4938.
[64] Y. Arima, H. Iwata, Effects of surface functional groups on protein adsorption and subsequent cell adhesion using self-assembled monolayers, J. Mater. Chem. 17 (2007) 4079–4087.
[65] Z. Tang, S.N. Sahu, M.A. Khadeer, G. Bai, R.B. Franklin, A. Gupta, Overexpression of the ZIP1 zinc transporter induces an osteogenic phenotype in mesenchymal stem cells, Bone 38 (2006) 181–198.
[66] M. Yamaguchi, M. Fukagawa, Role of zinc in regulation of protein tyrosine phosphatase activity in osteoblastic MC3T3-E1 cells: zinc modulation of insulin-like growth factor-I's effect, Calcified Tissue Int. 76 (2005) 32–38.